RL-TR-96-281
Final Technical Report
April 1997

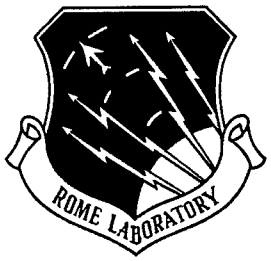

BEAM CONTROL IN DIFFRACTIVE SHORT-CAVITY QUANTUM WELLS FABRY-PEROTS FOR ADAPTIVE PROCESSING

Purdue University

David D. Nolte and M.R. Melloch

APPROVED FOR PUBLIC RELEASE; DISTRIBUTION UNLIMITED.

Rome Laboratory
Air Force Materiel Command
Rome, New York

This report has been reviewed by the Rome Laboratory Public Affairs Office (PA) and is releasable to the National Technical Information Service (NTIS). At NTIS it will be releasable to the general public, including foreign nations.

RL-TR-96-281 has been reviewed and is approved for publication.

APPROVED: George Brost

GEORGE A. BROST
Project Engineer

FOR THE COMMANDER: Gary D. Barmore

GARY D. BARMORE, Maj, USAF
Deputy Director
Surveillance & Photonics Directorate

If your address has changed or if you wish to be removed from the Rome Laboratory mailing list, or if the addressee is no longer employed by your organization, please notify RL/OCPA, 25 Electronic Pky, Rome, NY 13441-4515. This will assist us in maintaining a current mailing list.

Do not return copies of this report unless contractual obligations or notices on a specific document require that it be returned.

REPORT DOCUMENTATION PAGE

Form Approved
OMB No. 0704-0188

1. AGENCY USE ONLY *(Leave blank)*	2. REPORT DATE	3. REPORT TYPE AND DATES COVERED
	April 1997	**FINAL, Feb 95 - Jun 96**

4. TITLE AND SUBTITLE
BEAM CONTROL IN DIFFRACTIVE SHORT-CAVITY QUANTUM WELLS FABRY-PEROTS FOR ADAPTIVE PROCESSING

5. FUNDING NUMBERS
C - F30602-95-C-0016
PE - 62702F
PR - 4600
TA - P4
WU - PI

6. AUTHOR(S)
David D. Nolte, M.R. Melloch

7. PERFORMING ORGANIZATION NAME(S) AND ADDRESS(ES)
Purdue University
Department of Physics
West Lafayette IN 47907-1396

8. PERFORMING ORGANIZATION REPORT NUMBER

9. SPONSORING / MONITORING AGENCY NAME(S) AND ADDRESS(ES)
Rome Laboratory/OCPA
25 Electronic Pky
Rome NY 13441-4515

10. SPONSORING / MONITORING AGENCY REPORT NUMBER
RL-TR-96-281

11. SUPPLEMENTARY NOTES
Rome Laboratory Project Engineer: George A. Brost, OCPA, (315) 330-7669

12a. DISTRIBUTION AVAILABILITY STATEMENT
Approved for Public Release; Distribution Unlimited

12b. DISTRIBUTION CODE

13. ABSTRACT *(Maximum 200 words)*
Reflective photorefractive quantum well structures in the longitudinal-field geometry were demonstrated. A fully asymmetric Fabry-Perot device yielded an input diffraction efficiency of 10^{-3}. A novel photorefractive quarter-wave mirror was modeled. Performance similar to the asymmetric Fabry-Perot is predicted. Simulations of diffraction in multiple quantum well cavities shows mode coupling behavior.

14. SUBJECT TERMS
multiple quantum wells, photorefraction, asymmetric Fabry-Perot

15. NUMBER OF PAGES
30

16. PRICE CODE

17. SECURITY CLASSIFICATION OF REPORT	18. SECURITY CLASSIFICATION OF THIS PAGE	19. SECURITY CLASSIFICATION OF ABSTRACT	20. LIMITATION OF ABSTRACT
UNCLASSIFIED	**UNCLASSIFIED**	**UNCLASSIFIED**	**UNLIMITED**

Table of Contents

List of Figures

List of Tables

1. Introduction

Condensed matter optical microresonators display a wide variety of interesting behaviors and are suited to many applications. For example, the modification of electromagnetic modes in microcavity resonators is the basis for the design of semiconductor lasers [1-3] which rely on strong cavity quantum electrodynamic effects. Incorporation of an absorbing material within a cavity bounded by mirrors leads to modifications in both the amplitude and phase of the optical wave modes. A small number of modes of the optical field can be isolated with careful control of the cavity geometry and size. Other microcavity devices such as electro-optic modulators [4,5], SEEDs [6,7], and photorefractive multiple quantum wells [8-10] all utilize cavity effects, yet are not generally described in terms of microcavity resonators.

Photorefractive multiple quantum well devices are promising candidates for optical switches and have the advantages of high speed and low incident light intensity operation. As a consequence of the thickness of these structures, typically in the range of 1-4 μm, strong Fabry-Perot effects are present. A multiple quantum well microcavity sandwiched between unequal reflector interfaces can operate as a perfect absorber of light despite the fact that the thickness of the active region is only on the order of one absorption length. This is due to the microcavity effects which modify the optical modes and the density of states within the cavity such that the probability for absorption increases to unity. Photorefractive-induced index and absorption gratings cause additional modifications in the propagating optical modes and subsequent enhancement in photorefractive four-wave mixing performance.

Diffractive performance in these structures depends heavily on the orientation of the beams relative to the cavity surface. Modeling of photorefractive quantum well microcavities in various reflector geometries has yielded interesting resonance interactions possibly including mode-coupling and Rabi splitting. The diffraction efficiency of these devices operating in reflection can be enhanced above that obtained for anti-reflection-coated multiple quantum well devices where Fabry-Perot effects are not present. Careful control of the cavity dimensions yields quenching of the intensity of the zeroth order diffracted beam below that of the first order beam[9]. In principle, control of the relative magnitudes of the various diffracted orders may be achieved.

Alternative semiconductor microcavity structures promise to yield many interesting behaviors. A novel quarter-wave semiconductor mirror is predicted to have similar maximum diffractive performance to the photorefractive multiple quantum well Fabry-Perot devices without the associated insertion loss. Temperature tuning of the exction resonance

can also be used to explore the cavity-resonance enhancement effects predicted by numerical modeling.

2. Advancements in Device Processing

Most potential applications of the MQW ASFP's require improved surface quality. In particular, surface scatter can be a problem in imaging systems, such as for biomedical applications [11]. Several new chemical etching techniques were explored in order to achieve this goal. A pressurized chemical jet has been successfully used in other applications to achieve better surface quality [12]. We modified this chemical etching technique for use in an ultrasonic agitator. Since the agitator facilitates removal of the oxidized GaAs material, the standard chemical solution of 19 H_2O_2:1 NH_4OH did not have a high enough concentration of the oxidizer, H_2O_2. Several reagent ratios were examined in order to achieve optimum etching with the best performance coming from a solution of 66 H_2O_2:3 NH_4OH. Combined with ultrasonic agitation, this solution yields greatly improved surface quality and decreases surface scatter dramatically with the additional bonus of preferentially etching edges. For low temperature grown (LTG) devices this helps to remove any remaining non-insulating etch-stop material that might be left behind after standard processing. Unfortunately, this etching technique causes pinholes that, while unimportant in the transverse-field geometry, are fatal to the operation of the longitudinal-field devices. Additional studies of other etching techniques and/or solutions are needed to improve the surface quality of the longitudinal-field devices.

The use of titanium/gold contacts has shown promise in creating more uniform contacts by increasing the mechanical adhesion of the gold to the GaAs. Preliminary results in the transverse-field geometry showed that a square-wave AC applied field yields no electro-optic signal in devices with Ti/Au contacts, indicating symmetric contacts. Sine-wave fields yield the usual electro-optic response. Unfortunately, further studies showed that while a larger electro-optic response was generated in devices with Ti/Au contacts, the device-to-device uniformity was not as consistent as we had hoped. In order to circumvent these problems, several alternative methods of device fabrication and testing were examined, including thermal tuning of the exciton resonance, and terracing of a single sample with a single set of electrodes into sections of different thicknesses.

A new processing technique has also been developed for the longitudinal-geometry devices to improve their response to electric fields [13]. This process combines mesa-etching of the edges of the devices as well as placement of one electrical contact on a mesa of GaAs.

3. Longitudinal-Field-Geometry Devices

The fabrication of a large area longitudinal-field device requires more detailed processing than a transverse-field device to prevent electric field breakdown. LTG multiple quantum wells have been utilized to achieve a working longitudinal-field device with no non-semiconductor layers. The advent of new growth techniques has led to the ability to grow GaAs at low temperatures with good quantum confinement of the excitons [14]. LTG GaAs is semi-insulating as grown [15]. This is an advantage over standard temperature grown (STG) material which, because of the 3-4 μm thickness of a longitudinal-field device, is more difficult to make fully semi-insulating. LTG material also has a higher breakdown threshold and therefore lower leakage currents than STG GaAs. LTG MQWs coupled with the new fabrication technique dramatically increase the ability to hold off large electric fields of 100 kV/cm.

3.1. Shallow Quantum Wells

Initial device characterization was performed on a structure consisting of shallow $Al_{0.06}Ga_{0.94}As/Al_{0.16}Ga_{0.84}As$ quantum wells. The shallow quantum wells provide high-mobility vertical transport and sufficient quantum confinement for a strong electro-optic response, but do not produce a Stark shift. The device yields a differential transmission of nearly 100% for an applied field of 100 kV/cm as shown in Fig. 1.

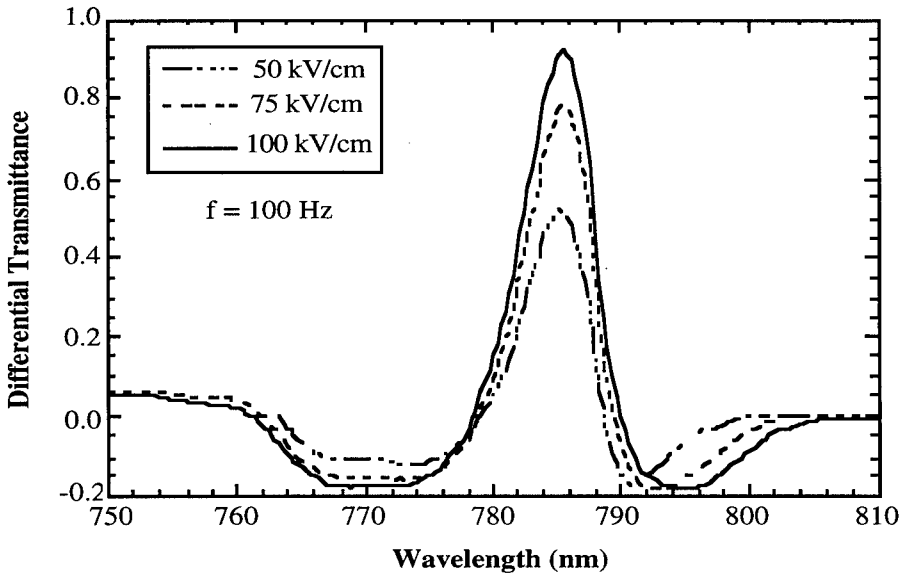

Fig. 1 Differential transmittance vs. wavelength for a longitudinal-field shallow quantum well device with a 100 Hz square wave applied field.

We fabricated shallow quantum well fully-asymmetric Fabry-Perot devices with high reflectors of gold, but shorting of the p-i-n region through pinholes hampered the performance of the device. The gold reflector may also have played a role in screening the space-charge field that is developed within the device.

3.2. Quantum Confined Stark Effect MQW ASFPs

At high fields the QCSE yields larger electro-optic effects than the field-broadening responsible for the electro-optic response of the shallow quantum wells. In order to take advantage of the larger electro-optic effects, a LTG longitudinal-field quantum-confined Stark effect (QCSE) device was grown. The structure consists of GaAs/$Al_{0.30}Ga_{0.70}As$ quantum wells with LTG $Al_{0.5}Ga_{0.5}As$ buffers [13].

3.2.1. Hybrid Transmission/Reflection Geometry

Fig. 2 shows results on the QCSE device operating in the glass-first hybrid transmission/reflection geometry [8]. A differential transmittance of 25% and a differential reflectance of 4% were obtained for a 100 Hz square-wave applied field of 50 kV/cm.

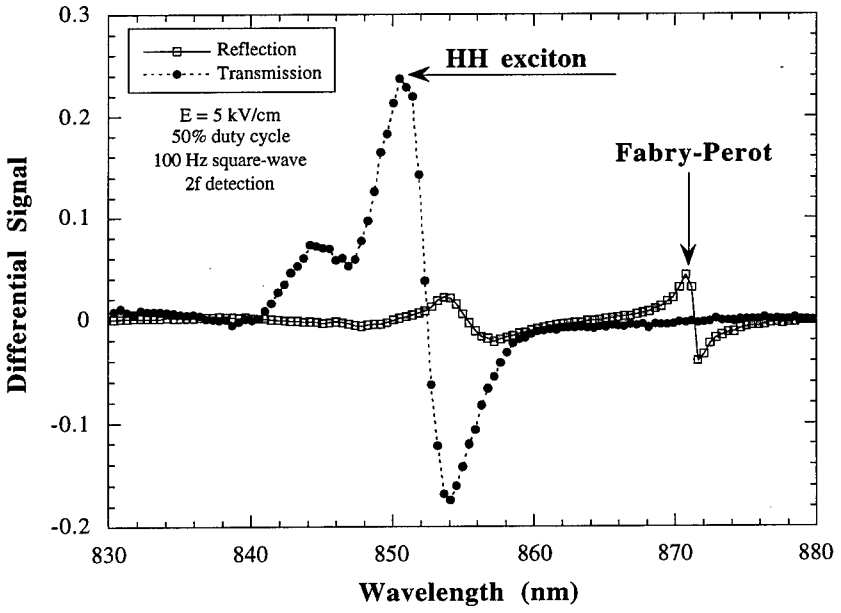

Fig. 2 Differential reflectance and transmittance vs. wavelength for a quantum-confined Stark effect photorefractive multiple quantum well with all beams incident glass-first.

The results of degenerate four-wave mixing experiments for the glass-first incident geometry are shown in Fig. 3.

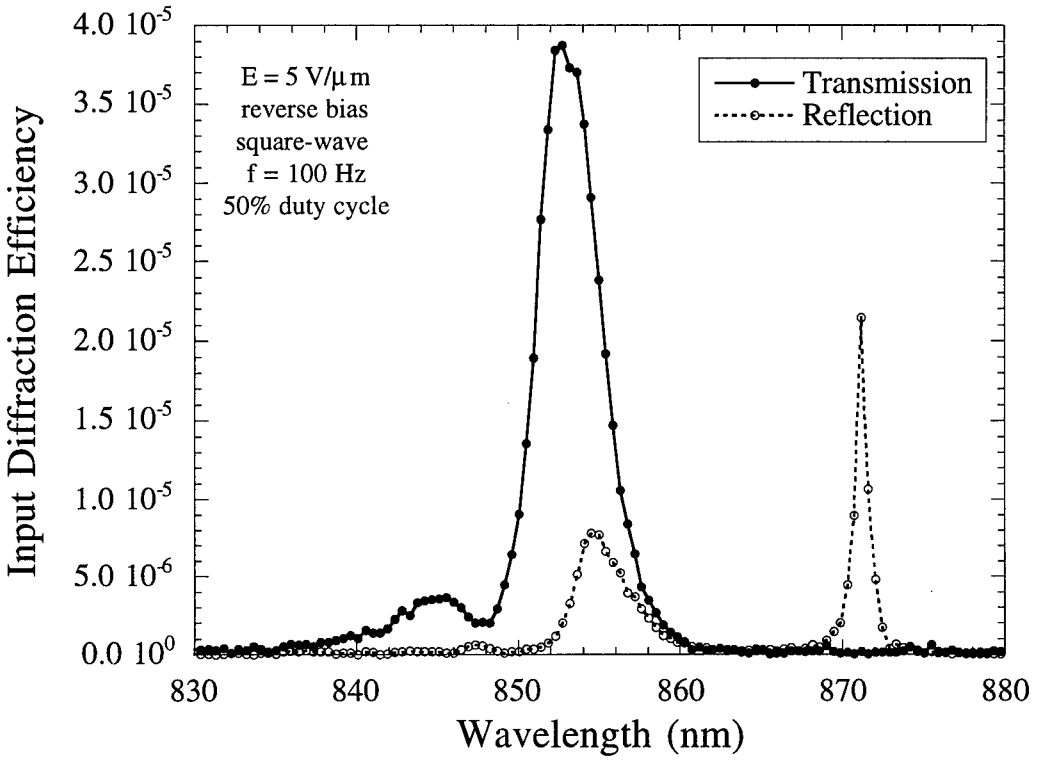

Fig. 3 Reflection and transmission intput diffraction efficiency vs. wavelength for the hybrid QCSE ASFP.

An output diffraction efficiency in reflection of $1x10^{-4}$, shown in Fig. 4, was obtained at an applied field of 75 kV/cm. The hybrid device shows a four-fold enhancement of the diffraction efficiency near the heavy-hole exciton at a field frequency of 1.4 kHz. A comparable, frequency independent, output diffraction efficiency is seen at the 871.5 nm Fabry-Perot resonance due to the near zero-reflectivity condition achieved at that wavelength.

This is the first demonstration of operation in reflection for a longitudinal-field geometry PR-MQW device. The low diffraction efficiency and differential reflectance are attributed to non-ideal field response and a Fabry-Perot resonance located 27 meV from the heavy-hole exciton. Such large Stark shifts are not attainable at the low applied field strengths of 50 - 75 kV/cm used in the experiments.

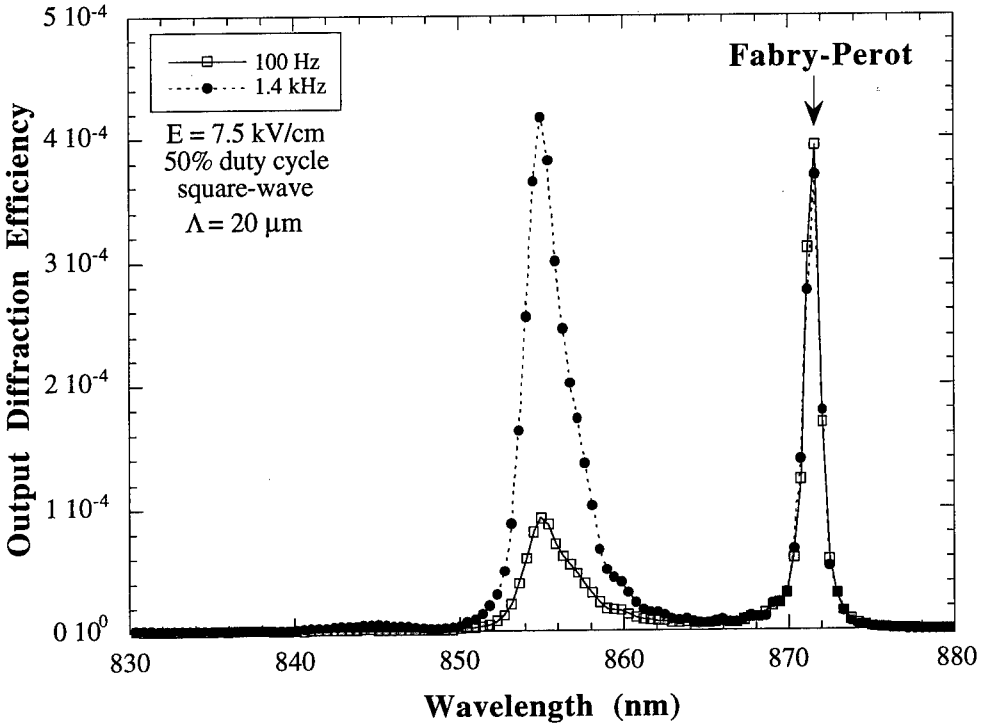

Fig. 4 Reflection output diffraction efficiency vs. wavelength as a function of field frequency for the hybrid QCSE device.

Several problems with device fabrication, resulting in low device yield, are still to be addressed. These include strain, shorting through pinholes, and contact technology. New processing techniques which may alleviate these problems are currently under investigation. We expect that refinements in processing techniques will lead to higher device performance by increasing device yield and allowing the application of larger electric fields.

3.2.2. Fully Asymmetric Fabry-Perot

The deposition of a high reflectivity dielectric coating allows operation in a fully asymmetric Fabry-Perot configuration. Numerical simulations show that ultimately, a QCSE fully asymmetric Fabry-Perot MQW device should yield the highest input diffraction efficiency for a MQW device [10]. Fig. 5 shows the diffractive performance of the fully asymmetric QCSE geometry device operating in reflection.

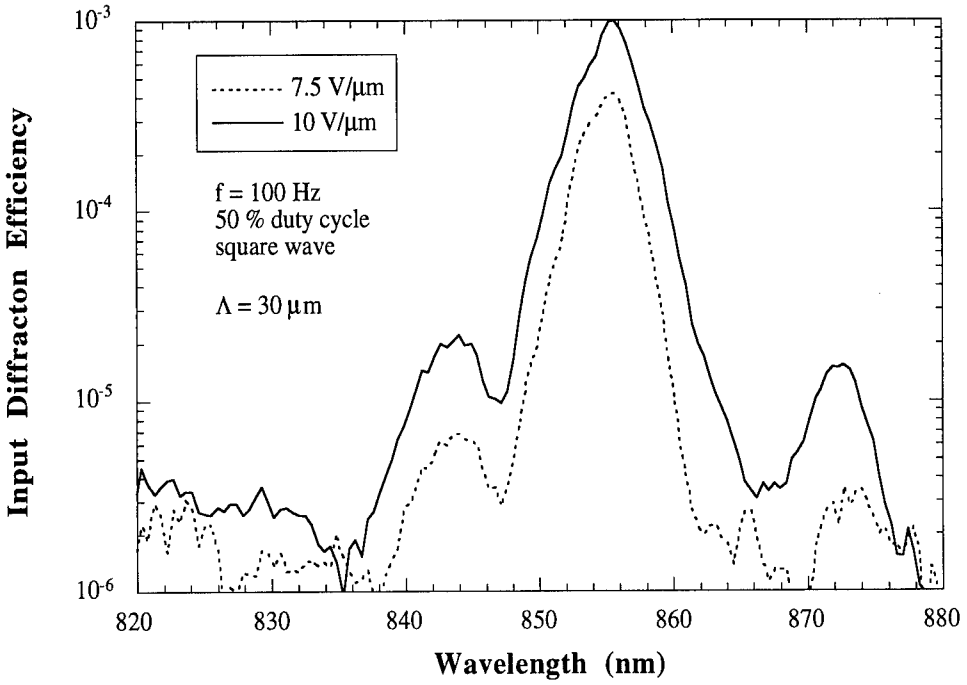

Fig. 5 Experimental degenerate four-wave mixing input diffraction efficiency vs. wavelength for a QCSE fully asymmetric MQW.

The diffraction efficiency is more than an order of magnitude below the best predicted performance. Explanations for this may include field screening by the dielectric coating and electrical shorting. Related work has shown enhanced diffractive performance in longitudinal devices operating in a transient time response mode[13]. No significant transient time response has been seen in our reflection devices. Ongoing work is examining possible explanations.

4. Semiconductor Microcavities

4.1. Quarter-wave Semiconductor Mirror

To date, the largest predicted diffraction efficiencies for photorefractive multiple quantum wells (MQWs) have been for longitudinal-field quantum-confined Stark effect devices utilizing the multiple beam interference effects of asymmetric Fabry-Perots (ASFPs)[10]. We have modeled a novel alternative device, a quarter-wave semiconductor mirror, that yields similar theoretical diffractive performance to ASFP's without much of the associated insertion loss. A quarter-wave photorefractive mirror operates in a high reflectivity region and does not require the careful control of surface quality and Fabry-Perot resonance placement necessary for optimum operation of a MQW ASFP. The

device, shown in Fig. 6, is similar in construction to stratified volume holographic optical elements [16,17] except that it consists of alternating quarter-wave optical thickness layers of a non-absorbing spacer and a photorefractive material.

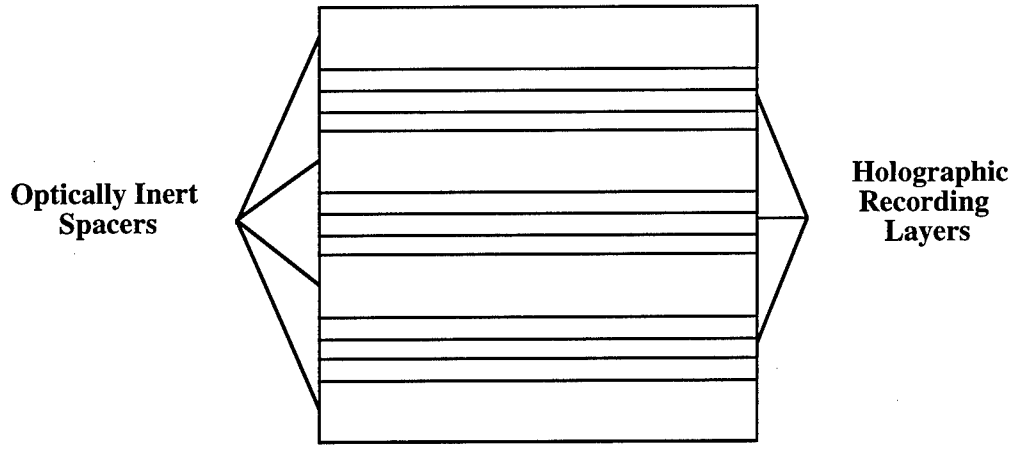

Fig. 6 Structure of a quarter-wave semiconductor mirror.

The longitudinal-field quarter-wave mirror modeled here is made up of AlAs spacers and photorefractive layers each consisting of several GaAs/$Al_{0.3}Ga_{0.7}As$ MQWs. Such a device would retain the speed and ultra-low light power requirements of photorefractive MQWs without the need for epitaxial lift-off or substrate etching.

4.1.1. Transfer Matrix Theory

The reflectivity of the quarter-wave mirror is modulated by the field-induced changes in absorbance and refractive index of the MQW layers, and was calculated using the transfer matrix method [18], extended for use with absorbing layers[19]. In this method, a matrix is defined for each material interface. Successive multiplication of the layers allows calculation of the reflectance of the device. The following matrices describe the AlAs/GaAs substrate interface (A), the AlAs/MQW interface (B), and the air/AlAs interface (C).

$$A = \frac{1}{2}\begin{bmatrix} \exp(ik_1a)\,(1 + {}^{k_1}/_{k_2}) & \exp(-ik_1a)\,(1 - {}^{k_1}/_{k_2}) \\ \exp(ik_1a)\,(1 - {}^{k_1}/_{k_2}) & \exp(-ik_1a)\,(1 + {}^{k_1}/_{k_2}) \end{bmatrix}$$

$$B = \frac{1}{2}\begin{bmatrix} \exp(ik_2b)\,(1 + {}^{k_2}/_{k_1}) & \exp(-ik_2b)\,(1 - {}^{k_2}/_{k_1}) \\ \exp(ik_2b)\,(1 - {}^{k_2}/_{k_1}) & \exp(-ik_2b)\,(1 + {}^{k_2}/_{k_1}) \end{bmatrix}$$

$$C = \frac{1}{2}\begin{bmatrix} \exp(ik_1 a)\,(1 + k_1/k) & \exp(-ik_1 a)\,(1 - k_1/k) \\ \exp(ik_1 a)\,(1 - k_1/k) & \exp(-ik_1 a)\,(1 + k_1/k) \end{bmatrix}$$

Here, the k_i's are given by

$$k_i = 2\pi n_i/\lambda - i\alpha_i/2$$

The matrix multiplication proceeds as

$$M = CB(AB)^{N-1}$$

where N is the number of Bragg stack periods. The reflectivity of the device is given by

$$R = |M_{21}/M_{11}|^2$$

where the matrix M has components

$$M = \begin{pmatrix} M_{11} & M_{12} \\ M_{21} & M_{22} \end{pmatrix}$$

A Stark shift of -20 meV/(100 kV/cm)^2 corresponding to $\Delta\alpha = 3300\text{cm}^{-1}$ was used in the simulations. Other parameters are given in Table I. Index changes were calculated from the absorption changes through the Kramers-Kronig relations. Since the total device thickness is on the order of 2 - 4 μm, the diffraction efficiencies were calculated in the Raman-Nath regime following the method of Ref # 10.

Heavy Hole	**Light Hole**	**Continuum**
$\alpha_{HHo} = 9000\ \text{cm}^{-1}$	$\alpha_{LHo} = 4000\ \text{cm}^{-1}$	$\alpha_{Co} = 8000\ \text{cm}^{-1}$
$\Delta\alpha_{HH} = -3300\ \text{cm}^{-1}$	$\Delta\alpha_{LH} = -1400\ \text{cm}^{-1}$	$\Delta\alpha_{C} = 0.000\ \text{cm}^{-1}$
$\Omega_{HHo} = 1.475$ eV	$\Omega_{LHo} = 1.490$ eV	$\Omega_{Co} = 1.475$ eV
$\Delta\Omega_{HH} = -0.020$ eV	$\Delta\Omega_{LH} = -0.020$ eV	$\Delta\Omega_{C} = 0.000$ eV
$\Gamma_{HHo} = 0.0035$ eV	$\Gamma_{LHo} = 0.0045$ eV	$\Gamma_{Co} = 0.0060$ eV
$\Delta\Gamma_{HH} = 0.0020$ eV	$\Delta\Gamma_{LH} = 0.0025$ eV	$\Delta\Gamma_{C} = 0.0020$ eV

Table I. Quantum-confined Stark effect MQW parameters used for modeling of a photorefractive quarter-wave mirror.

4.1.2. Theoretical Results

Fig. 7 shows reflective and 1st-order diffractive performance for the quarter-wave mirror described above with AlAs and MQW layer thicknesses yielding a center wavelength, λ_o, of 845 nm. Although the field-induced reflection modulation is not large at the operational wavelength of 845 nm, the presence of index and absorption gratings causes a 20% decrease in the reflectivity. Peak diffraction efficiency occurs at a 30% reflectivity condition, rather than at the anti-reflection condition for an ASFP.

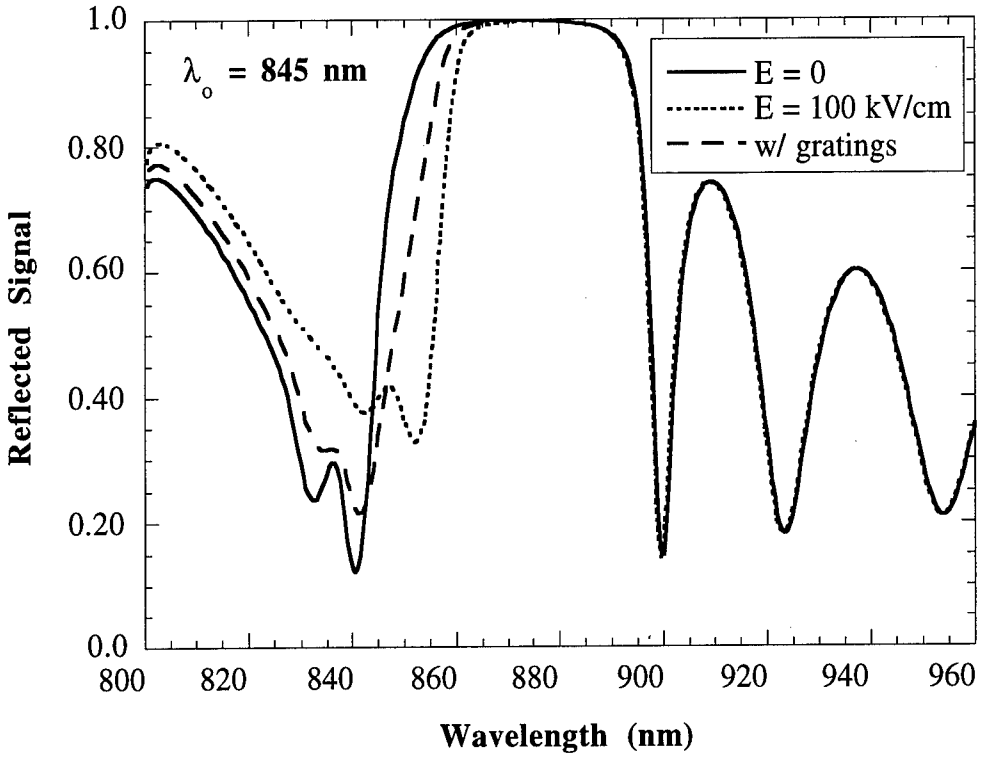

Fig. 7 Calculated reflectance under zero and maximum applied field (dashed lines) and in the presence of photorefractive gratings (solid line) for a 30 period mirror consisting of AlAs spacers and $GaAs/Al_{0.3}Ga_{0.7}As$ MQWs centered at λ_o = 845 nm.

A first order, or input, diffraction efficiency of 2%, shown in Fig. 8, is predicted. This diffraction efficiency is comparable to that predicted for a QCSE ASFP operating in reflection.

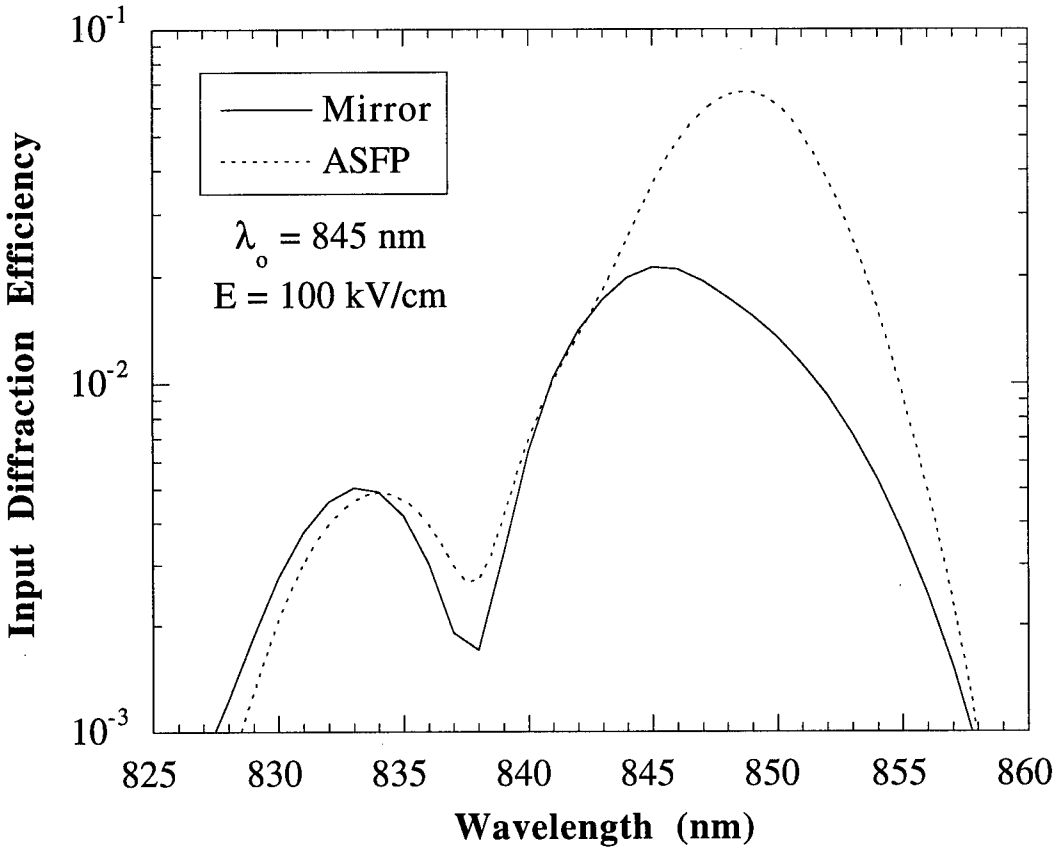

Fig. 8 Simulated input diffraction efficiency vs. wavelength for a photorefractive quarter-wave mirror and a QCSE ASFP.

The input diffraction efficiency is relatively constant over a large range of the mirror center wavelength as shown in Fig. 9. As a result, small variations in refractive index due to uncertainties in aluminum fraction during growth of the layers have little effect on mirror diffractive performance. Systematic shifts in the mirror period are also not as critical as in standard distributed Bragg reflectors since the operational bandwidth is relatively large. A final advantage of this device would be that substrate removal and etching to obtain a favorable cavity resonance are not required. Preliminary experimental examination of this type of device is currently underway.

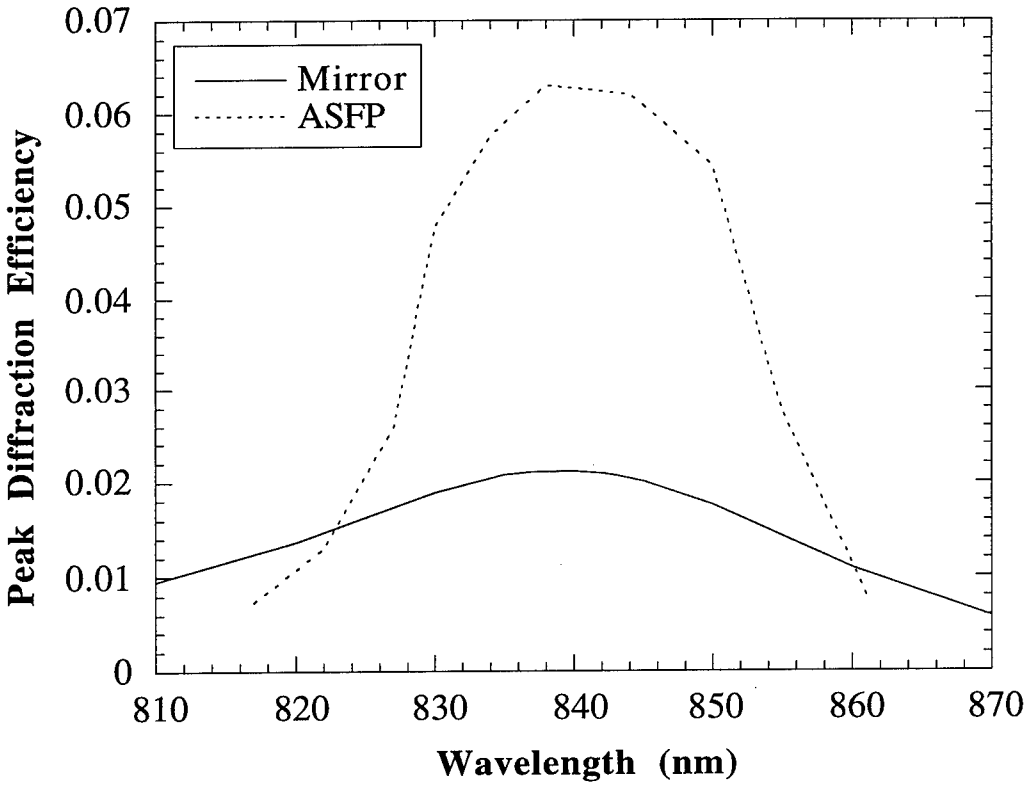

Fig. 9 Maximum calculated input diffraction efficiency vs. wavelength for quarter-wave mirrors of various center wavelengths and ASFPs at various cavity resonance conditions.

4.2. Resonance Interactions

Semiconductor planar microcavities are optoelectronic structures in which the quantization of both electronic and electromagnetic modes must be considered on equal footing[20]. Normal-mode coupling between exciton modes and cavity modes in short cavities produces Rabi splitting of the exciton-cavity resonances, which is observable in the reflection and transmission spectra of high-Q cavities[21]. In this section, we describe dynamic holography experiments on low-Q cavities [10] that possess many of the features of normal-mode coupling. In addition to enhancing the diffraction efficiency from these devices, residual normal mode coupling may be observable in the diffraction spectra. Semiconductor asymmetric planar microcavities exhibit enhanced diffraction in dynamic holography when the cavity resonance is tuned near the exciton resonance. The enhancement is a residual effect, in these low-Q cavities, of normal-mode coupling and Rabi splitting.

4.2.1. Asymmetric Short-Cavity Fabry-Perots

An asymmetric short-cavity Fabry Perot [10], also called a "half"-cavity [22], is a thin film with a high-reflector on one face, and the natural reflectance of the semiconductor surface on the other. Because of the low surface reflectivity of GaAs (30%), these asymmetric cavities are low-Q cavities, and have not been considered as "microcavities" with observable coupling between cavity and exciton modes. However, we show here that when performing dynamic holography in reflectance on these low-Q cavities, it may be possible to identify the individual photon and exciton branches, and to identify a normal-mode splitting that is comparable to the Rabi splitting observed in high-Q cavities.

A numerical simulation of the diffracted signal in reflectance from an asymmetric bulk GaAs cavity is shown in Fig. 10 along with a schematic identifying the photon and exciton branches. The contour scale is logarithmic, demonstrating an order of magnitude enhancement of the diffraction near the crossing condition. The sample thickness, around 1 micron, is macroscopic by microcavity standards, but two distinct diffraction maxima are observable when the cavity resonance is tuned close to the excitonic transition wavelength. The splitting between these peaks is on the order of 10 - 15 meV (Ω = 400 - 600 fsec), which is comparable to the vacuum Rabi splitting calculated from Savona *et al* [23]. Therefore, although the residence time of the photon in this bulk low-Q cavity is only 20 - 40 fsec, normal-mode coupling and splitting should still be identifiable experimentally in the cw four-wave mixing spectra. Because of the high sensitivity of four-wave mixing to nuances in the dielectric function, this splitting may even be observable at room temperature in low-Q multiple quantum well cavities.

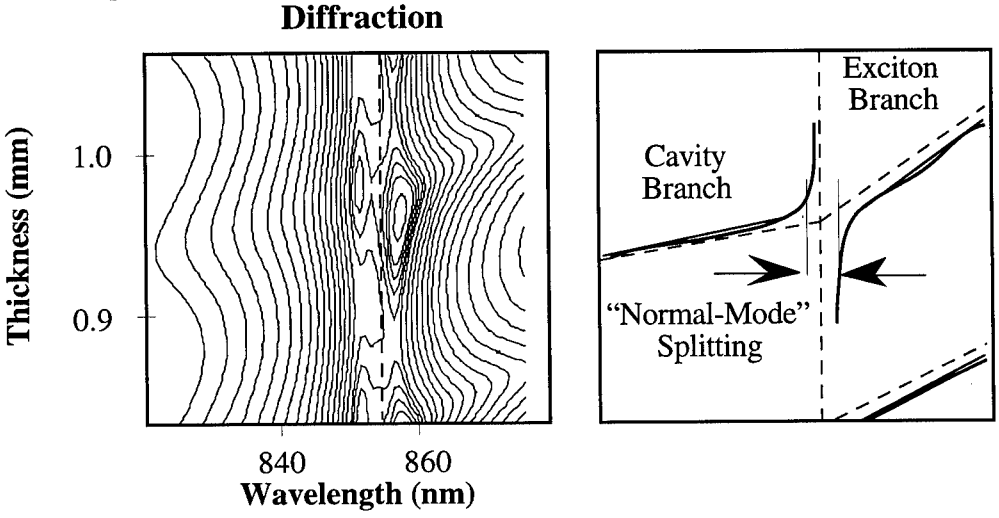

Fig. 10 Simulated diffraction vs. wavelength and thickness for a low-Q bulk GaAs "half" (or asymmetric) microcavity. The normal-mode diagram is shown for comparison.

4.2.2. Temperature-Tuning the Cavity

The effects of different resonance conditions on diffractive performance have been investigated experimentally in a 2.3 μm-thick transverse-field asymmetric Fabry-Perot consisting of low temperature growth GaAs/AlAs multiple quantum wells coated on one side with a highly reflective dielectric stack[9]. The temperature-dependent band gap shift of the multiple quantum wells is utilized to tune the excitonic resonance with respect to the cavity resonance. The reflectances vs. wavelength for this device at two different temperatures are shown in Fig. 11a. At 85 K the Fabry-Perot appears to be at an on-resonant condition, while at 175 K it is detuned from resonance.

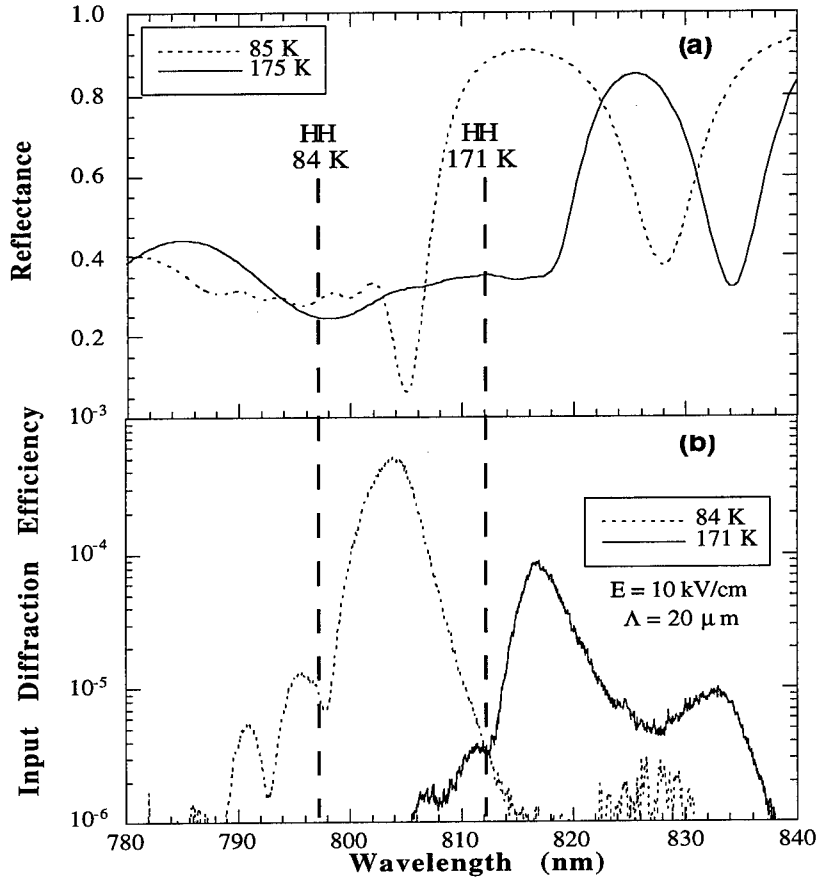

Fig. 11 (a) Experimental reflectances vs. wavelength of a LTG transverse-field geometry GaAs/AlAs multiple quantum well microcavity at two different cavity resonance conditions. (b) Input diffraction efficiencies vs. wavelength. The dashed lines indicate the position of the heavy hole excitons at the two temperatures.

The results of non-degenerate four-wave mixing experiments conducted at 84 K and 171 K are shown in Fig. 11b, displaying nearly an order of magnitude difference in the diffraction efficiency at the two resonance conditions. While the diffraction spectra vary in magnitude, they have qualitatively similar shapes, suggesting that the mode-tuning is a weak function of the temperature shift. Factors influencing the magnitude of the diffraction efficiency include cavity-induced enhancement, due to a shift from an on-resonance to an off-resonance condition, as well as thermal broadening of the excitonic transition. The secondary peak in the input diffraction efficiency to the high-energy side of the maxima at both temperatures is suggestive of residual mode splitting effects and is on the order of calculated splittings [23]. Diffraction enhancement is also seen at the low-energy cavity resonance 30-40 meV from the main diffraction peak. A study over a higher temperature range is shown in Fig. 12. The spectral shape of the input diffraction efficiency varies as the resonances shift with respect to each other. The maximum diffraction of 10^{-4} occurs at 829 nm for the 220 K curve.

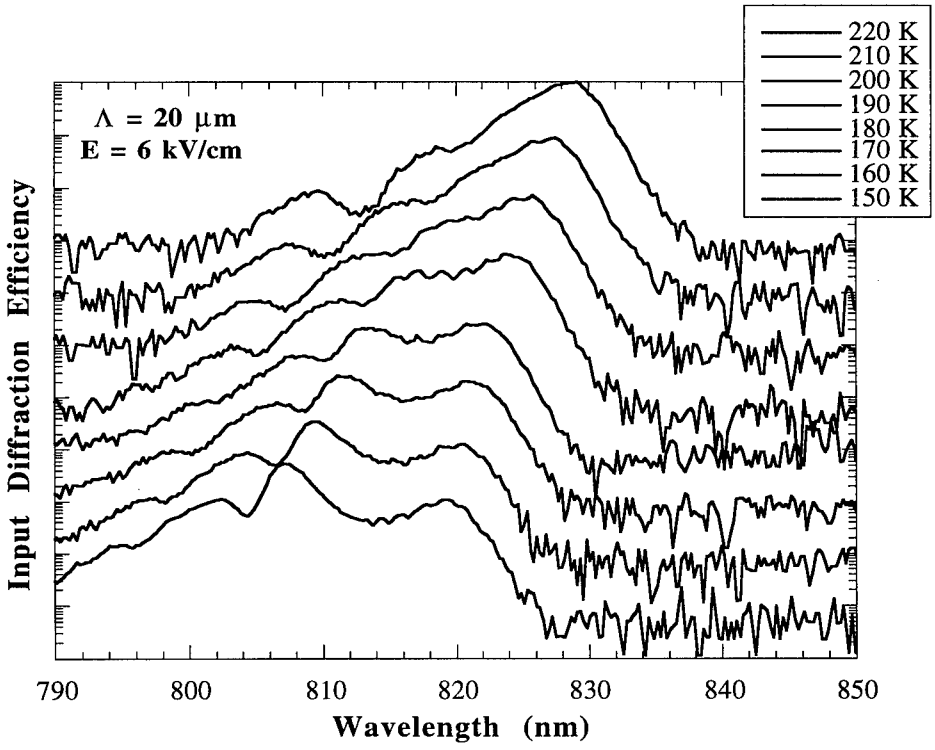

Fig. 12 Degenerate four-wave mixing vs. wavelength and temperature for an LTG AlAs-barrier MQW coated with a dielectric reflector. Each curve is offset from the next by one order of magnitude to display spectral features.

4.2.3. Terraced Devices

Terraced devices have also been fabricated in order to study the resonance interactions under identical field conditions. Terracing is achieved through chemical etching of the non-absorbing spacer on one side of the MQW region. The reflectance of such a device consisting of an LTG GaAs/AlAs MQW transverse-field geometry "half" cavity with four terraces is shown in Fig. 13. Each terrace is illuminated individually in order to examine a single configuration of the dual resonances.

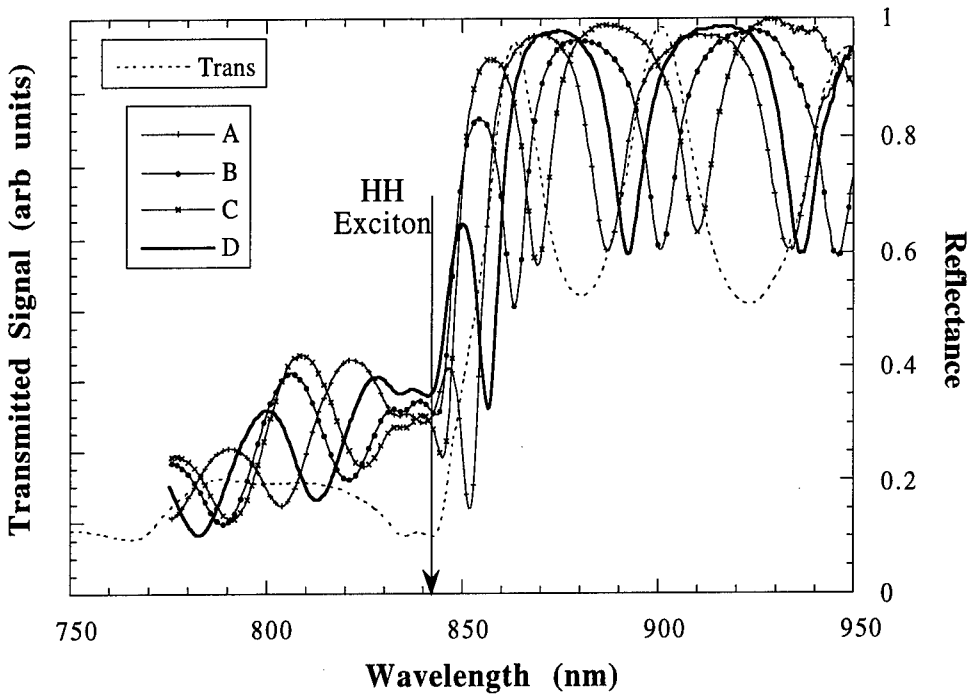

Fig. 13 Reflectance vs. wavelength for each terrace (A, B, C, D) on a transverse-field geometry MQW "half" cavity. Transmittance of this MQW structure without the dielectric reflector shows the position of the excitons.

The four terraces yield different resonance conditions that affect the non-degenerate four-wave mixing performance as shown in Fig. 14. Terrace "A" appears to yield the best input diffraction efficiency. The lineshape of the diffraction changes also changes as the cavity resonance is shifted with respect to the exciton resonance.

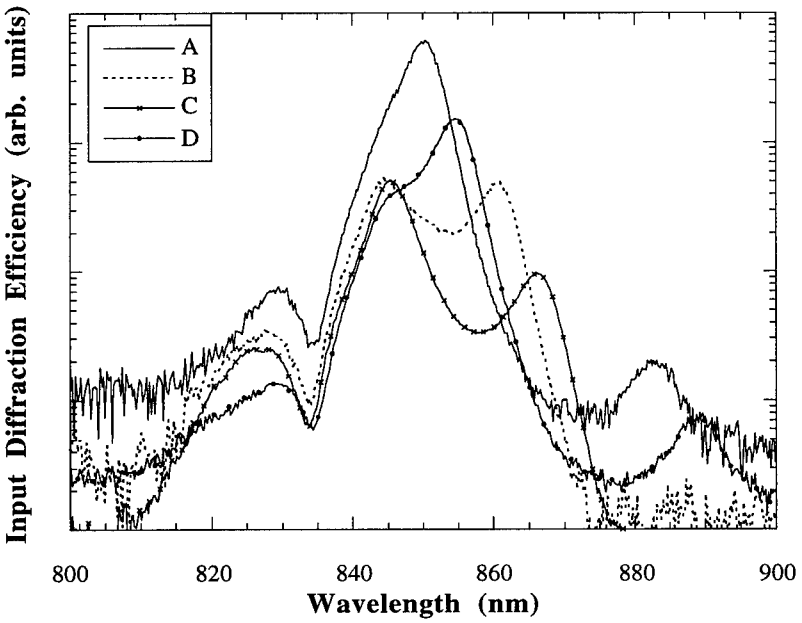

Fig. 14 Input diffraction efficiency vs. wavelength on four distinct terraces (A, B, C, D) on a transverse-field LTG MQW coated with a dielectric reflector.

5. Discussion and Future

In conclusion, we have demonstrated the first operation of longitudinal-field geometry MQWs in reflection. A hybrid QCSE device yielded a nearly a 6-fold enhancement of the output diffraction efficiency in reflection. A fully asymmetric QCSE device yielded an input diffraction efficiency of 10^{-3}. Several issues still remain regarding the fabrication and transient time response of these devices. We have also described how the asymmetric Fabry-Perots can be viewed as microcavity devices with many potentially interesting behaviors. Modeling of a novel device, the photorefractive quarter-wave mirror, predicted similar performance to the ASFP. This mirror would require significantly simplified device processing as compared to the ASFP and is predicted to be relatively insensitive to uncertainties or fluctuations in growth parameters. Similar structures which utilize microcavity effects hold the promise of additional novel performance characteristics. Simulations of diffraction in MQW cavities shows mode coupling behavior. Rabi splitting may also be observable in these devices. Temperature tuning of the exciton transition and terracing of the cavities has allowed more detailed study of the resonance effects on the diffractive performance. A cavity with sharper room temperature excitons, as can be obtained with stoichiometric GaAs quantum wells, may allow the best resolution of mode interactions and Rabi splitting.

This work was performed with the support of the United States Air Force Rome Laboratory.

Bibliography

1. F. DeMartini and G. R. Jacobovitz, "Anomalous spontaneous-stimulated-decay phase transition and zero-threshold laser action in a microscopic cavity," Phys. Rev. Lett. **60**, 1711 (1988).
2. H. Yokayama, K. Nishi, T. Anan, Y. Nambu, S. D. Brorson, E. P. Ippen, and M. Suzuki, Opt. Quantum Electron. **27**, 1347 (1992).
3. Y. Yamamoto and S. Machida, "Microcavity semiconductor laser with enhanced spontaneous emission," Phys. Rev. A. **44**, 657 (1991).
4. R. H. Yan, R. J. Simes, L. A. Coldren, and A. C. Gossard, "Transverse modulators with a record reflection change of >20%/V using asymmetric Fabry-Perot structures," Appl. Phys. Lett. **56**, 1626 (1990).
5. K. H. Calhoun and N. M. Jokerst, "AlGaAs/GaAs thin-film Fabry-Perot modulator on a glass substrate by using alignable epitaxial lift-off," Opt. Lett. **18**, 882-884 (1993).
6. K-K. Law, R. H. Yan, L. A. Coldren, and J. L. Merz, "Self-electro-optic device based on a superlattice asymmetric Fabry-Perot modulator with an on/off ratio > 100:1," Appl. Phys. Lett. **57**, 1345 (1990).
7. P. Zouganeli, R. J. Grindle, A. W. Rivers, G. Parry, and J. S. Roberts, "Symmetric self-electro-optic effect device using symmetric-cavity quantum well electroabsorption modulators," IEEE Phot. Tech. Lett. **6**, 939 (1994).
8. K. M. Kwolek, M. R. Melloch, and D. D. Nolte, "Dynamic holography in a reflection/transmission photorefractive quantum-well asymmetric Fabry-Perot," Appl. Phys. Lett. **65**, 385 (1994).
9. K. M. Kwolek, M. R. Melloch, and D. D. Nolte, "Photorefractive asymmetric Fabry-Perot quantum wells: transverse-field geometry," Appl. Phys. Lett. **67**, 736 (1995).
10. D. D. Nolte and K. M. Kwolek, "Diffraction from a short-cavity Fabry-Perot: application to photorefractive quantum wells," Opt. Comm. **115**, 606 (1995).
11. S. C. W. Hyde, N. P. Barry, R. Jones, J. C. Dainty, P. M. W. French, M. B. Klein, and B. A. Wechsler, "Depth-resolved holographic imaging through scattering media by photorefraction," Opt. Lett. **20**, 1331 (1995).

12. H. Tanobe, T. Tamanuki, T. Uchida, F. Koyama, and K. Iga, "Spray Selective etch Process for Short-Cavity Fabrication of GaAs/GaAlAs Surface Emitting Laser," Jpn. J. Appl. Phys. **31**, 949 (1992).
13. I. Lahiri, M. Aguilar, D. D. Nolte, and M. R. Melloch, "High-efficiency Stark-geometry photorefractive quantum wells with intrinsic cladding layers," Appl. Phys. Lett. **68**, 517 (1996).
14. I. Lahiri, D. D. Nolte, E. S. Harmon, M. R. Melloch, and J. M. Woodall, "Ultrafast-lifetime quantum wells with sharp exciton spectra," Appl. Phys. Lett. **66**, 2519 (1995).
15. A.C. Warren, J. M. Woodall, P. D. Kirchner, X. Yin, F. Pollak, and M. R. Melloch, "Role of excess As in low-temperature-growth GaAs," Phys. Rev. B **46**, 4617 (1992).
16. R. De Vre and L. Hesselink, "Analysis of photorefractive stratified volume holographic optical elements," J. Opt. Soc. Am. A **11**, 1800 (1994).
17. G. P. Nordin, R. V. Johnson, and A. R. Tanguay, "Diffraction properties of stratified volume holographic elements," J. Opt. Soc. Am. A **9**, 2206 (1992).
18. A. Yariv and P. Yeh, *Optical Waves in Crystals* (John Wiley & Sons, New York, 1984).
19. F. Bretenaker, L. Zibell, J. P. Pocholle, E. Barbier, and M. Papuchon, "GaAs/Ga1-xAlxAs Bragg reflectors at absorption wavelengths," Opt. Comm. **71**, 129 (1989).
20. P. R. Berman, "Cavity Quantum Electrodynamics," in *Advances in Atomic, Molecular, and Optical Physics* (Academic Press, Boston, 1994).
21. C. Weisbuch, M. Nishioka, A. Ishikawa, and Y. Arakawa, "Observation of coupled exciton-photon mode splitting in a semiconductor quantum microcavity," Phys. Rev. Lett. **69**, 3314 (1992).
22. A. Tredicucci, Y. Chen, V. Pellegrini, M. Borger, L. Sorba, F. Beltram, and F. Bassani, "Controlled exciton-photon interaction in semiconductor bulk microcavities," Phys. Rev. Lett. **75**, 3906 (1995).
23. V. Savona, L. C. Andreani, P. Schwendimann, and A. Quattropani, "Quantum well excitons in semiconductor microcavities: unified treatment of weak and strong coupling regimes," So. St. Comm. **93**, 773 (1995).

☆U.S. GOVERNMENT PRINTING OFFICE: 1-97-509-127-47178

MISSION OF ROME LABORATORY

Mission. The mission of Rome Laboratory is to advance the science and technologies of command, control, communications and intelligence and to transition them into systems to meet customer needs. To achieve this, Rome Lab:

a. Conducts vigorous research, development and test programs in all applicable technologies;

b. Transitions technology to current and future systems to improve operational capability, readiness, and supportability;

c. Provides a full range of technical support to Air Force Material Command product centers and other Air Force organizations;

d. Promotes transfer of technology to the private sector;

e. Maintains leading edge technological expertise in the areas of surveillance, communications, command and control, intelligence, reliability science, electro-magnetic technology, photonics, signal processing, and computational science.

The thrust areas of technical competence include: Surveillance, Communications, Command and Control, Intelligence, Signal Processing, Computer Science and Technology, Electromagnetic Technology, Photonics and Reliability Sciences.